STATISTICS, OPTIMIZATION AND INFORMATION COMPUTING
Stat., Optim. Inf. Comput., Vol. **14**, November 2025, pp 2329–2354.
Published online in International Academic Press (www.IAPress.org)

SBPar Scanning: Toward a Complete Optimal Skeleton Scan Strategy for Additive Manufacturing

Nadir RIHANI[1] , Iatimad AKHRIF[1], Mostapha El JAI[1,2,*]

[1]*Euromed University of Fes, UEMF, Fez, Morocco*
[2]*Mechanic, Mechatronic and Command Laboratory, ENSAM-Meknes, Moulay Ismail University, Marjane 2, Al-Mansour, Meknes, Morocco*

Abstract In a previous work (Prog Addit Manuf 6:93–118, 2021), a novel Additive Manufacturing scan strategy was designed; the Skeleton-Based Perpendicular (SBP) scanning should show minimal trajectory series compared to classical exiting hatching patterns used in the literature. In contrast, this pattern should lead to mechanical anisotropy due to the one-way oriented printing if it is applied in all part's layers; a complementary scan strategy must be designed to balance the SBP orientations. This important constraint led the author of this paper to develop the "Skeleton-Based Parallel" (SBPar) strategy as a SBP's complementary scan for avoiding such issues. Subsequently, the present work details the design of the SBPar pattern and the corresponding scan length; analytical formulations are drawn-up for a simple rectangle as a proof of the concept. Therefore, the superposition of SBP and SBPar constitutes the total skeletal scanning (SB). Results emphasized two conflictual interests: apart from stripe scan, the proposed SBPar scan exhibits a maximized trajectory compared to the other scan strategies; thus, it seems lastly compromising the minimization objective targeted by SBP scan. On the other hand, according to this maximization aspect, the second interest is regarded in terms of surface control which requires maximizing matter spreading and thereafter offering higher densification to the processed surfaces. Furthermore, The SB and the classical scan strategies showed degrees of length-similarities according to decision variables adopted herein. Further works will be dedicated to the implementation of the Skeletal-Based trajectory within real 3D-parts and then to the associated mechanical characterization.

Keywords Additive Manufacturing; Hatching strategy; Skeleton-Based Perpendicular scanning; Skeleton-based Parallel scanning; Scan Optimization

DOI: 10.19139/soic-2310-5070-1917

1. Introduction

Similarly to all fabrication technologies, Additive Manufacturing (AM) process parameters are considered among the most decisive variables to be controlled during fabrication [1, 2, 3]; the robustness of given process parameters levels is also of great consideration since some parameters' values naturally imply stable output behavior than others, especially in terms of both centering and dispersion criteria, or more generally in terms of Signal-to-Noise ratios [1, 4, 5, 6]. In this regard, AM scanning strategies are no exception [7]. Indeed, in AM technologies, among number of inputs, hatching strategies are the set of local geometry characteristics that are mostly affecting the local properties of printed parts [8, 9, 10, 11, 12, 13, 14, 15]. Novel and more complex scanning strategies have also been developed recently like fractal scan strategies based on Hilbertand and Peano-Gosper curves [14].

A scan strategy comprises the pattern style [16, 17], the hatch space and the orientation [17, 18], and so forth [19]. Researchers found that the resulting mechanical properties in 3D-printed parts are straightforward affected

*Correspondence to: Mostapha El JAI (Email: m.eljai@ueuromed.org). Euromed University of Fes, UEMF, Fez, Morocco.

ISSN 2310-5070 (online) ISSN 2311-004X (print)

by the hatch strategies in terms of processed matter density [20, 21, 22], residual stress [23, 24, 25], heat effect [25, 26, 27], and more specifically the mechanical anisotropy [24, 28, 29, 30, 31, 32]. Hence, it the majority of situations, further post-fabrication treatments are required for smoothening physical and metallurgical properties so that the printed parts can show characteristics consensus between the technical requirements; this is, indeed, the role of post-heat treatment [27, 33, 34] and Hot Isostatic HIP for instance [35, 36, 37]. Moreover, scan strategy was found to be conditioning roughness levels particularly with regard to the hatch space values and layer thickness [38, 39] and is necessarily condoning the post-finishing operations [40].

According to another perspective, number of authors discussed the need of minimizing scan trajectory in order to save time, matter, or processing energy [19, 65]; in the other hand, trajectory optimization issue is one of the major consideration in mechanics in general such as in robotics, control planning, and for the related energy saving [17, 41, 42, 43, 44]. This paper presented rigorous mathematical formulations of the scan lengths of 5 different patterns; four of them are classically used in the literature and in the industry namely chessboard, stripe, spiral, and contour hatching patterns [8, 9, 10, 11, 12, 13, 14]; while the fifth corresponds to Skeleton Based Perpendicular (SPB) scan which was designed for saving production time [17, 19]. The SBP pattern was designed by EL Jai et al at the basis of the skeleton of 2D-shape notion [19]; the skeleton was defined as a hypothetical feature that is regarded as the lieu of in-shape points that are the nearest from the shape borders [45]. The mathematical skeleton feature was first defined as a topological species of shapes [45, 46]; It also represents a physical or virtual object for the reconstitution of any form and the corresponding construction could be carried out using number of techniques, but all can be clustered in the realm of the algorithmic geometry and then into the computational geometry [47, 48, 49, 50, 51]; therefore, the skeleton found its straightforward application on image processing and shape recognition [52, 53]. Recently, El Khattabi et al proposed a skeleton based clustering algorithm as a perspective of their works [54, 55]. It is then worth mentioning that the proposed design will take advantages of existing mathematical tools of multi-objective optimization in order to try to optimize number of conflictual outcomes [56, 57, 58, 59, 60, 61, 62]. Statistical modeling will be also of high importance since not all geometric features could be modeled in an analytical way; hence number of regression models (linear and non-linear) [63, 64, 58, 2, 38, 44] will be useful to understand the behavior of the geometric features of the new scan strategy according to the input parameters that are listed in the rest of the development.

Based on the above discussion, the present article is the second one of a series of works that are dedicated to the integration of the skeletal scan paths. In the first paper [19], the authors developed the SPB hatching pattern as a likely-minimal path compared to classical strategies. In this work, the author proposes an SPB complementary scan, namely the Skeleton Based Parallel scanning, the SBPar pattern. The present concept corresponds to the superposition of the SBP and SBPar patterns inasmuch as they are presenting couple of orthogonal patterns, one on the other. That is to say, the complete Skeleton Based (SB) scan pattern is constituted of the pair SBP ; SBPar as the basis of a novel scan strategy dedicated to additive manufacturing; as a proof of concept, it is proposed to study a simple rectangle, but with variable dimensions and variable hatch space. A special attention is hence given to the gain or save of length of the proposed design compared to classical scan strategies. Hence, the author displays in detail the geometry parametrization of the proposed scan, the mathematical length formulation and the corresponding performance indicator developed in here for comparing the SBPar and SB total scans to classical AM scan strategies.

The rest of the paper presents the Mathematical development in section 2. This section meticulously exhibits the geometry parameters, and the detail of scan lengths. This section also depicts the adopted gain of length indicators and the benchmark hatching strategies alike. As for the benchmark analysis, the study considered two main perspectives; the minimization/maximization of length but also the length similarity percentages or feasibility as adopted by the author; section 3 depicts the corresponding computations, curves, parametric surfaces and the related modeling, statistics, discussion and analysis; section 4 concludes the work by highlighting the most significant findings with the corresponding analysis. Perspectives are in fine introduces the next works of this series of Skeleton Based scanning for AM integration.

2. Mathematical development of the total scan length

This works aims to exhibit a rigorous analytical description of the total scan length of the proposed SBPar scan trajectory; thereafter, the proposed SBPar pattern will be combined to the SBP scan strategy that was developed by El Jai et al [19]. This combination constitutes the primary pair of layers used to build a given parallelepiped as a simple part being used as the proof of the concept of the proposed scan technique that is based on the skeleton of 2D shapes. In order to widen the analysis and the computations, variate dimensions of the rectangle are handled namely the length L1 and the width L2. The hatch space of the hypothetic scan is also got as a computation input and decision variable of the analysis. In another hand, since the SBPar scan is to be combined to the previous SBP scan strategy, readers are referred to the previous article [19] which exhibits the detailed approach of the SBP scan and the associated scan strategies adopted in the benchmark of the present study. Then, this section is divided in three main parts:

- subsection 2.1 depicts the geometrical parameterization of the SBPar scan pattern of "$(L_1, L_2)_{(L_1>L_2)}$" rectangle which is used as the proof pf concept of this new scan strategy;
- subsections 2.2 to 2.5 address step-by-step the scan length equations starting from the scan tracks equations (subsection 2.2), passing by the formalization of the summation of these matter that constitute the total scan lengths of the areas 1 to 3; the total SBPar length equation is then exhibited in subsection 2.5;
- Finally, subsection 2.4 presents the Specific Gain of length per surface unit (SG) that is exploited for peer-to-peer scan length comparison leading to a rigorous the benchmark according to the proposed parametrization and hatch space distance "e".

All codes' implementation, computations, and plots were carried out by matlab 2021a.

2.1. SBPar pattern and parametrization

SBPar pattern is based on a series of scans dedicated to a rectangle (L_1, L_2) surface filling knowing a priori hatch space "e". Figure 1 displays the SBPar pattern principle proposed in this study which completes the SBP scan developed by El Jai et al exhibited in Figure 2 [19]. Subsequently, Figure 3.a) to 3.c) depict the corresponding geometry parameters handled in the mathematical development of subsections 2.2 to 2.5. The parametrization distinguishes three zones denoted Area 1, Area 2, and Area 3 that define in fine the total scan length.

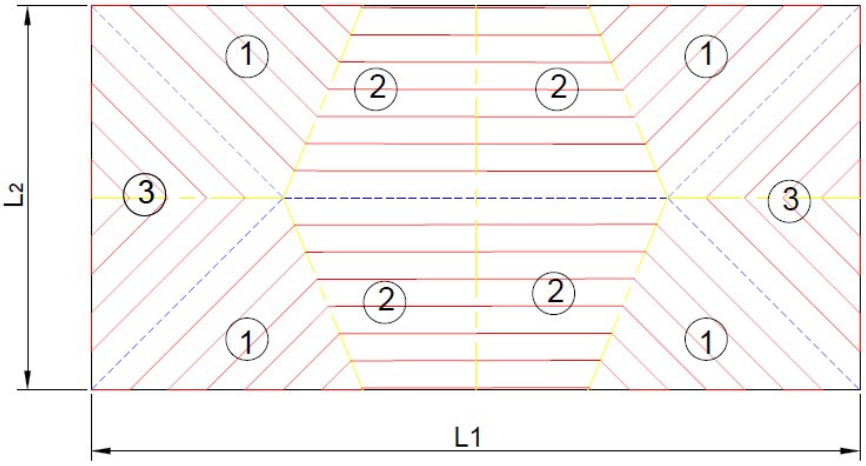

Figure 1. Main pattern and areas decomposition {1, 2, 3} of the SBPar scanning strategy

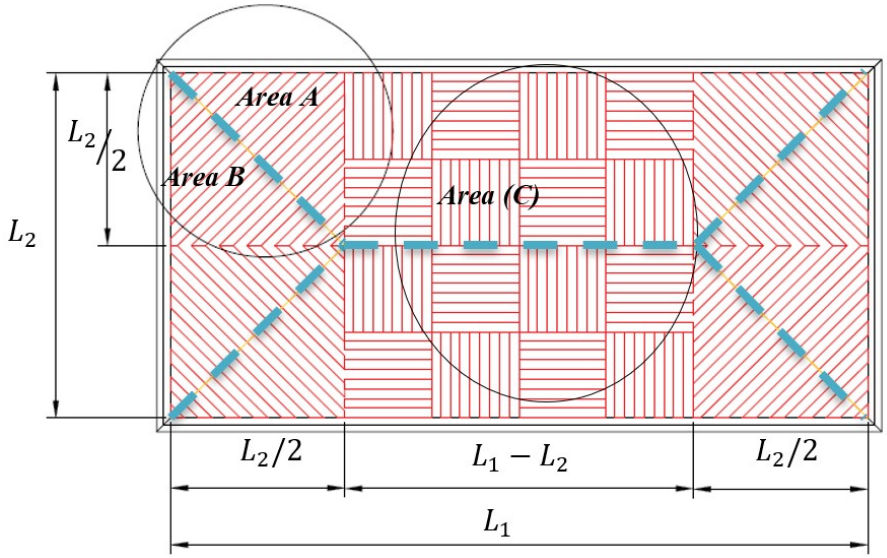

Figure 2. Skeleton Based Perpendicular (SBP) pattern [19]

According to the horizontal and vertical symmetries of the rectangle and the scan trajectory, one can easily prove that the calculation of the scan lengths can be restricted on areas 1, 2, and 3 at one of the rectangle's quarters and multiplied by the number of symmetries to obtain the total trajectory length. Thereby, the related geometry parameters and objects are defined for the northeastern corner as listed in the following points:

- Area 1: set of points $\{A_1, A_2, A_3, C_i, H_{1i}\}$ and the set of angles $\{\theta_1, \theta_2, \theta_3\}$ (Figure 3.a to 3.c);
- Area 2: set of points $\{A_2, A_3, A_5, A_6, A_7, H_{1i}, H_{2i}\}$ and the set of angles $\{\theta_3, \theta_4\}$ (Figure 3.a, Figure 4);
- Area 3: set of points $\{A_1, A_3, A_4, A_{1i}, A_{3i}, \theta_1\}$ (Figure 5);

The scanning jumps expressing the hatch space are assigned by the variable "e" as it is displayed in Figure 3.c, Figure 4, and Figure 5.

2.2. SBPar Scanning length and total skeletal scan length

This subsection exhibits the stepwise construction of the lengths series in Areas 1, 2, and 3 of the SBPar scanning patterns according to the parametrization developed in section 2.1 of the manuscript. According to Figure 3, one can notice that the key point of the distance analysis is to determine initially the coordinates of the points A2, A3 that are defined by the system (1). These points detection allowed computing the scanning lengths in all rectangles areas that are proposed in Figure 3, where the next sections exhibit the stepwise formulation of the total scanning lengths in the areas 1, 2, and 3 depicted in Figure 1.

$$\begin{cases} \{A_1\} & = (B_1) \cap (D_2) \\ \{A_2\} & = (D_1) \cap (\Delta) \end{cases} \tag{1}$$

Such that (s.t.):

(B_1) is the bisector of the obtuse angle $(\widehat{A_1})$
$(D_2) = \{(x, y) : y = 0\}$
$(D_1) = \{(x, y) : y = {}^{L_2}/_2\}$
(Δ) is the bisector of the obtuse angle $(\widehat{A_3})$

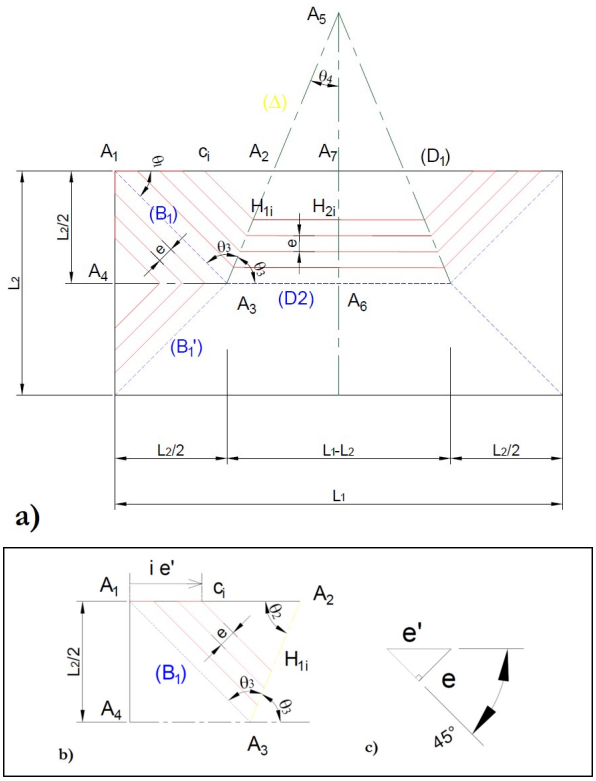

Figure 3. Parametrization of the SBPar scanning strategy a) Global view b) Local parametrization of the area A c) Hatch space (jump gap) parameter

2.3. Scanning lengths' series

The scanning series are defined herein as the basis lines that the summation constitutes the total scanning length. Thus, subsection 2.3 builds the stepwise scanning length series formulations; while section 2.4 and 2.5 presents the summation of these latter for total SBPar scanning length computing that is developed in section 3.

2.3.1. Area 1 :
Since $A_1A_2A_3$ is a known triangle, the angles $(\theta_1, \theta_2, \theta_3)$ are thus defined since at least the angle $(\widehat{A_1})$ is known equal to $\pi/2$ and A_1A_3 are also known.

Thus

$$\forall(C_i, H1i) : \frac{C_iH_{1i}}{\sin\theta_2} = \frac{C_iA_2}{\sin\theta_3} = \frac{A_1A_2 - A_1C_i}{\sin\theta_3}$$

$$\Rightarrow C_iH_{1i} = (A_1A_2 - A_1C_i)\frac{\sin\theta_2}{\sin\theta_3}$$

s.t:

$$\begin{cases} A_1C_i & = ie' \text{ (Fig.3.b)} \\ e' & = \sqrt{2}e \text{ (Fig.3.c)} \end{cases}$$

Thus, the series of (SBPar) scans C_i H_{1i} are defined by equation (2).

$$C_iH_{1i} = (A_1A_2 - i\sqrt{2}e)\frac{\sin\theta_2}{\sin\theta_3} \tag{2}$$

Where i is the index of the scan as it is depicted in Figure 3.a and 3.b.

2.3.2. Area 2 :

Figure 4 geometrically defines the scan lengths' series of the Area 2. The total scanned length of Area 2 corresponds to the sumation of the $H_{1i}\ H_{2i}$ distances. Thus, according to Figure 4:

$$\frac{H_{1i}H_{2i}}{H_{2i}A_5} = \tan\theta_4 = \tan\left(\frac{\pi}{2} - \theta_3\right) = \frac{1}{\tan\theta_3}$$

$$H_{1i}H_{2i} = \frac{H_{2i}A_5}{\tan\theta_3}$$

$$H_{2i}A_5 = A_5A_6 - ie$$

$$\text{Where } \tan\theta_3 = \frac{A_5A_6}{A_3A_6} \implies A_5A_6 = A_3A_6(\tan\theta_3)$$

$$\text{s.t. } A_3A_6 = \frac{L_1}{2} - \frac{L_2}{2} = \frac{1}{2}(L_1 - L_2)$$

$$\implies A_5A_6 = \frac{(L_1 - L_2)(\tan\theta_3)}{2}$$

$$H_{2i}A_5 = \frac{(L_1 - L_2)(\tan\theta_3)}{2} - ie$$

$$H_{1i}H_{2i} = \frac{L_1 - L_2}{2} - \frac{ie}{\tan\theta_3} \tag{3}$$

Hence, the scan lengths' series of the Area are defined by equation 3.

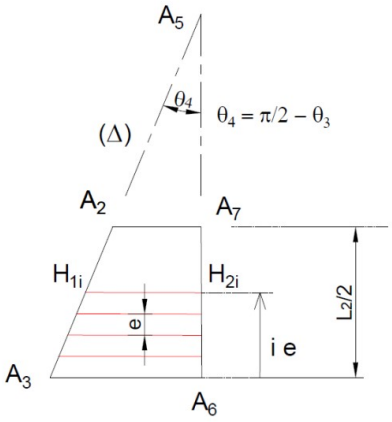

Figure 4. Parametrization of the Area 2

2.3.3. Area 3 :

The analysis of Figure 5 led to the definition of the scan lengths' series of Area 3 by means of equation A.

$$A_{1i}A_{3i} = A_1A_3 - 2ie \tag{4}$$

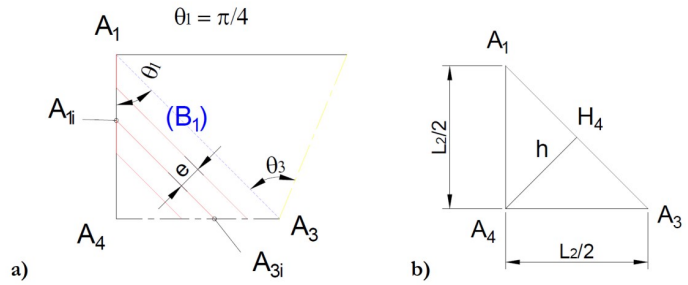

Figure 5. Parametrization of the Area 3 a) Parameters details b) Envelop points

2.4. SBPar Scanning Length Per Area

The total (SBPar) scan is to be computed as a combination of 5 main components as listed below:

- L_{A1}: Length corresponding to the trajectory scan of Area 1;
- L_{A2}: Length corresponding to the trajectory scan of Area 2;
- L_{A3}: Length corresponding to the trajectory scan of Area 3;
- L_{sk}: Length corresponding to the length of the skeleton itself;
- L_J: Total length corresponding to the jumps (hatch spaces).

Thus, the total (SBPar) scan length is defined by equation (5):

$$L_{SBPar} = 4(L_{A1} + L_{A2} + L_{A3}) + L_{sk} + L_J \tag{5}$$

2.4.1. Area 1 Total Length: L_{A1}

The total (SBPar) length of Area 1 is expressed by equation (6):

$$L_{A1} = \sum_{i=1}^{n} C_i H_{1i} \tag{6}$$

$$\text{s.t. } n = E\left(\frac{L_2}{2e}\right)$$

From equation (1), equation (6) becomes:

$$L_{A1} = \sum_{i=1}^{n} \frac{\left(A_1A_2 - i\sqrt{2}e\right)\sin\theta_2}{\sin\theta_3}$$

This led to the final expression of L_1 as described by equation (7):

$$L_{A1} = \frac{\left(nA_1A_2 - \frac{\sqrt{2}}{2}en(n+1)\right)\sin\theta_2}{\sin\theta_3} \tag{7}$$

2.4.2. Area 2 Total Length: L_{A2}

The total (SBPar) length of Area 2 is expressed by equation (8):

$$L_{A2} = \sum_{i=1}^{n} H_{1i}H_{2i} = \sum_{i=1}^{n}\left(\frac{(L_1 - L_2)}{2} - \frac{ie}{\tan\theta_3}\right)$$

Thus:

$$L_{A2} = \frac{n}{2}(L_1 - L_2) - \frac{e}{\tan\theta_3}\frac{n}{2}(n+1) \tag{8}$$

2.4.3. Area 3 Total Length: L_{A3}

The total (SBPar) length of Area 3, L_{A3}, is expressed by equation (9):

$$L_{A3} = \sum_{i=1}^{n'} A_{1i}A_{3i} = \sum_{i=1}^{n'} (A_1A_3 - 2ie) = n'A_1A_3 - \frac{2e}{2}n'(n'+1)$$

From Figure 4.b:

$$n' = E\left(\frac{h}{2}\right), \quad h = \frac{\sqrt{2}}{4}L_2$$

Thus:

$$L_{A3} = n'A_1A_3 - en'(n'+1) \tag{9}$$

2.4.4. Scan Jumps Total Length: L_J

According to Figure 1 of the manuscript, the jumps exist only in Areas 1 and 3, which correspond to two jump lengths components L_{J1} for Area 1 and L_{J3} for Area 3. Thus, the total length of jumps for the (SBPar) scan over the studied rectangle is expressed by equation (10) and then by means of equation (12):

$$L_J = L_{J1} + L_{J3} \tag{10}$$

s.t.

$$\begin{cases} L_{J1} = \sum_{i=1,i=i+2}^{n} e' = \sum_{i=1,i=i+2}^{n} \sqrt{2}e \approx \frac{\sqrt{2}}{2}en \\ L_{J3} = \sum_{i=1,i=i+2}^{n'} e' = \sum_{i=1,i=i+2}^{n'} \sqrt{2}e \approx \frac{\sqrt{2}}{2}en' \end{cases} \tag{11}$$

Hence:

$$L_J = \frac{\sqrt{2}}{2}e(n+n') \tag{12}$$

2.4.5. Skeleton Length: L_{sk}

According to Figure 1 and the horizontal and vertical symmetries, the skeleton length can be computed according to equation (13):

$$L_{sk} = 4(A_1A_3) + 2(A_3A_6) \tag{13}$$

Now let's find the expressions of the distances A_1A_3, A_1A_2, and A_3A_6:

$$\begin{cases} A_1A_3 = \sqrt{(x_3-x_1)^2 + (y_3-y_1)^2} & (14.1) \\ A_1A_2 = \sqrt{(x_2-x_1)^2 + (y_2-y_1)^2} & (14.2) \\ A_3A_6 = \sqrt{(x_6-x_3)^2 + (y_6-y_3)^2} & (14.3) \end{cases} \tag{14}$$

s.t. (x_1, y_1), (x_2, y_2), (x_3, y_3), and (x_6, y_6) are respectively the coordinates of the points A_1, A_2, A_3, and A_6.
From Figure 1 of the main text:

$$\begin{cases} x_1 = 0,\ y_1 = \frac{L_2}{2} \\ x_3 = \frac{L_2}{2},\ y_3 = 0 \\ x_6 = \frac{L_1}{2},\ y_6 = 0 \end{cases} \tag{15}$$

In addition, A_2 is defined by the system (1) as the bisector of the angle $\widehat{A_1A_3A_6}$. Thus, the following developments are based on the description of Figure 3.a) of the main text:

$$x_2 = (x_3 - x_1) + d$$

where:

$$\begin{cases} \tan\left(\frac{\pi}{2} - \theta_3\right) = \frac{d}{\frac{L_2}{2}} = \frac{1}{\tan\theta_3} \\ x_1 = 0 \end{cases}$$

$$\implies x_2 = x_3 + \frac{L_2}{2\tan\theta_3}$$

In addition:

$$\theta_1 + 2\theta_3 = \pi \implies \frac{\pi}{4} + 2\theta_3 = \pi \implies \theta_3 = \frac{3\pi}{8}$$

Thus:

$$\begin{cases} x_2 = \frac{L_2}{2}\left(1 + \frac{1}{\tan\theta_3}\right) \\ y_2 = \frac{L_2}{2} \end{cases} \tag{16}$$

Hence, according to equations (14) to (16):

$$\begin{cases} A_1A_3 = \frac{\sqrt{2}}{2}L_2 \\ A_1A_2 = \frac{L_2}{2}\left(1 + \frac{1}{\tan\theta_3}\right) \\ A_3A_6 = \frac{L_1 - L_2}{2} \end{cases} \tag{17}$$

Then, the total skeleton length can be expressed by equation (18):

$$L_{sk} = L_1 + (2\sqrt{2} - 1)L_2 \tag{18}$$

2.5. Compilation and Total SBPar Scanning Length

According to the above development, the SBPar total scanning length L_{SBPar} is computed according to equation (19.1) and system (19.2):

$$L_{SBPar} = 4(L_{A1} + L_{A2} + L_{A3}) + L_{sk} + L_J \tag{19.1}$$

$$\begin{cases} L_{A1} = n\frac{L_2}{2}\left(1 + \frac{1}{\tan\theta_3}\right) \\ L_{A2} = \frac{n}{2}(L_1 - L_2) - \frac{e}{\tan\theta_3}\frac{n(n+1)}{2} \\ L_{A3} = \frac{\sqrt{2}}{2}n'L_2 - en'(n'+1) \\ L_{sk} = L_2(2\sqrt{2} - 1) + L_1 \\ L_J = \frac{\sqrt{2}}{2}e(n + n') \\ n = E\left(\frac{L_2}{2e}\right),\ n' = E\left(\frac{L_2}{e\frac{\sqrt{2}}{4}}\right),\ \theta_3 = \frac{3\pi}{8} \end{cases} \tag{19.2}$$

Such that:

- L_{A1}: Area 1 total length
- L_{A2}: Area 2 total length
- L_{A3}: Area 3 total length
- L_J: Scan jumps total length
- L_{sk}: Skeleton length
- $E(x)$: Integer part of the given x variable

Since the SBPar strategy and the related length are formulated, it is interesting to sum up with the SBP scan length to derive a complete formulation of the skeletal scan strategy SB. Hence, the total skeletal length L_{SB} is given by expression (20):

$$L_{SB} = L_{SBP} + L_{SBPar} \tag{20}$$

L_{SBP} was formulated according to the pattern of Figure 2, which depends on the hatch space, the lengths L_1 and L_2, and the levels decomposition of the area C [19]. For further details, readers are referred to the Appendix of El Jai et al. paper [19].

2.6. Comparison and Benchmark Method

In this investigation, a benchmark study is adopted to position the proposed SBPar scan within the existing literature scan frames. The strategies adopted in this work are:

- Chess pattern: denoted by the index "ch" and of length L_{ch};
- Stripe pattern: denoted by the index "st" and of length L_{st};
- Spiral pattern: denoted by the index "sp" and of length L_{sp};
- Contour pattern: denoted by the index "cont" and of length L_{cont}.

The SBP strategy will also be compared to the new SBPar. The benchmark strategies patterns are summarized in Table 1.

In another hand, the total scan lengths of the benchmark strategies $\{L_{ch}, L_{st}, L_{sp}, L_{cont}\}$ are detailed in the Appendix of the SBP work [19]. in this paper, the benchmark analysis was conducted using the specific gain of scan length. In this paper, the same indicator will be handled in order to compare gain (positive) or loss (negative) of length between two competing strategies. General speaking, the specific gain (SG) of length between two scan strategies i and j for a given rectangle $(L_1 \times L_2)$ is expressed by equation (21). In this expression, the lengthL_i is considered as a reference length to which the L_{SBPar} is be compared.

$$SG_i\left(\%\text{ per mm}^2\right) = \frac{(L_{SBPar} - L_i)}{L_i}\frac{1}{L_1 L_2}$$

or

$$SG_i\left(\%\text{ per mm}^2\right) = \left(\frac{L_{SBPar}}{L_i} - 1\right)\frac{1}{L_1 L_2} \tag{21}$$

It is worth denoting that the dimensions $(L_1, L_2)_{(L_1 > L_2)}$, of the rectangle are varied during the computations to evaluate the length gain according to the shape's dimensions. L_1 and L_2 are varied according to the procedure in equation (22), such that:

$$\begin{cases} L_1(i) = 100 + 10 \times i & \text{for } i \in \{1, \ldots, 20\} \quad (22.1) \\ L_2(j) = 50 + 10 \times j & \text{for } j \in \{1, \ldots, 20\} \quad (22.2) \\ \text{if } L_1(i) > L_2(j): & A(i,j) = L_1(i) \times L_2(j) \quad (22.3) \\ \text{else:} & A(i,j) = \text{NaN} \end{cases} \tag{22.4}$$

Thus:

$$L_1(i) \in [100, 300], \quad L_2(j) \in [50, 250] \tag{23}$$

In this work, the specific gains (SGs) are expressed for each competing scan strategy as depicted in system (24):

$$\begin{cases} SG_{ch}\left(\%\text{ per mm}^2\right) = \left(\frac{L_{SBPar}}{L_{ch}} - 1\right)\frac{1}{L_1 \times L_2} \\ SG_{st}\left(\%\text{ per mm}^2\right) = \left(\frac{L_{SBPar}}{L_{st}} - 1\right)\frac{1}{L_1 \times L_2} \\ SG_{sp}\left(\%\text{ per mm}^2\right) = \left(\frac{L_{SBPar}}{L_{sp}} - 1\right)\frac{1}{L_1 \times L_2} \\ SG_{cont}\left(\%\text{ per mm}^2\right) = \left(\frac{L_{SBPar}}{L_{cont}} - 1\right)\frac{1}{L_1 \times L_2} \\ SG_{SBP}\left(\%\text{ per mm}^2\right) = \left(\frac{L_{SBPar}}{L_{SBP}} - 1\right)\frac{1}{L_1 \times L_2} \end{cases} \tag{24}$$

such that SG_{ch}, SG_{st}, SG_{sp}, SG_{cont}, and SG_{SBP} are respectively the specific length gains regarding chess, stripe, spiral, contour, and finally the SBP patterns compared to the SBPar pattern. Furthermore, the same computations and analysis were carried out for the total skeletal-based scan L_{SB} compared to the other scan strategies. In that case, two layers $\{L_{SBP} + L_{SBPar}\}$, constituting the L_{SB}, should be compared to two consecutive layers of a given competing scan pattern; hence, the SG indicator in the case of the total skeletal scan

Benchmark Hatching Pattern	Representation and Parametrization According to [19]
Chessboard (chess)	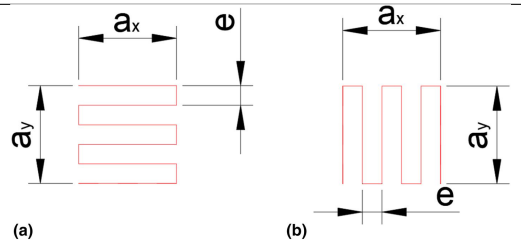
Stripe	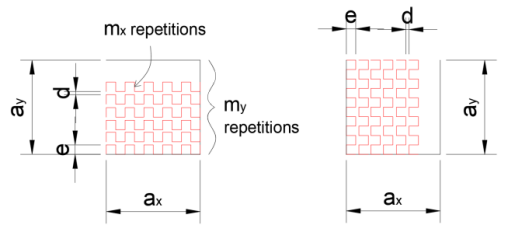
Spiral	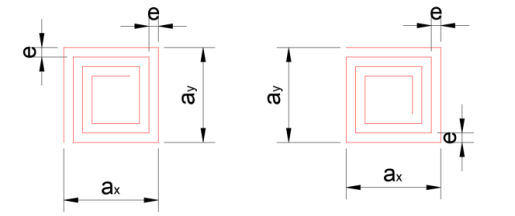
Contour	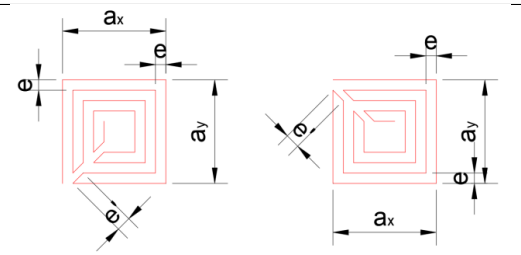

Table 1. Benchmark strategy display

(SB) is additionally computed according to expression (25), while L_{SB} is given by equation (3) and L_i expresses the length of the competing strategies {chess, stripe, spiral, contour} developed previously [19].

$$SG_{SB,i}\left(\%\,\text{per mm}^2\right) = \left(\frac{L_{SB}}{2L_i} - 1\right)\frac{1}{L_1 \times L_2} \tag{25}$$

It is worth recalling that the aim of the present analysis is to figure out how the rectangle dimensions (L_1, L_2) and hatch space affect the total length of the $SBPar$ and SB patterns and whether the scanned trajectories are maximized or minimized compared to the benchmark scan patterns. Therefore, the SG indicators were designed to answer two main needs:

- Computing and characterizing both $SBPar$ and SB patterns feasibilities that are expressed by the negativeness of the SG indicators; a negative SG means that the proposed scan strategies minimize the hatching circulation compared to another competing scan strategy. In contrast, positive values of SG indicate skeletal scan maximization. At this level, it is noteworthy that either minimizing or maximizing

the trajectory is not considered as optimization objectives themselves. In other words, this work primarily aims at characterizing the gain of length per surface unit as a function of the geometry parameters instead of a proper optimization of the length; this latter will be reached by a simple analysis of L_{SBPar} length, which revealed a special behavior according to the decision variables, as will be exhibited in the next sections.
- An arbitrary choice of "SG negativeness" will lead to evaluating the feasibility of this condition regarding each competitive scan strategy separately. Subsequently, a special consideration is assigned to the percentage of feasibility as a general index for scan patterns competitiveness discussion, respectively for L_{SBPar} and L_{SB}.

Based on the above, the feasible space describing the competitiveness of the $SBPar$ and total skeletal scan SB strategies can be respectively derived according to expressions (26) and (27).

Based on the above, the feasible space describing the competitiveness of the $SBPar$ and total skeletal scan SB strategies can be respectively derived according to expressions (26) and (27):

Based on the above, the feasible space describing the competitiveness of the $SBPar$ and total skeletal scan SB strategies can be respectively derived according to expressions (26) and (27):

$$(L_1^*, L_2^*, e^*) = \arg(SG_{SBPar,i} < 0) \tag{26}$$
$$(L_1^{**}, L_2^{**}, e^{**}) = \arg(SG_{SB,i} > 0) \tag{27}$$

Such that (L_1^*, L_2^*, e^*) and $(L_1^{**}, L_2^{**}, e^{**})$ express the (L_1, L_2, e) values according to which respectively L_{SBPar} and L_{SB} are showing lower scan trajectory compared to the benchmark scan strategies.

Furthermore, a pairwise L_{SB} similarity to the benchmark scan strategies has been carried out, expressing the closeness of $SG_{SB,i}$ to the zero line, meaning that the difference of SB length to another scan strategy length is likely equal. To assess this, the error of similarity or similarity tolerance ε, ranging between 10^{-6} and 10^{-4}, has been adopted, and the similarity percentage has been computed according to the number of data around this value, according to expression (28):

$$\text{Sim}(\%) = \frac{\text{card}(\arg(|SG_{SB,i} - 0| < \varepsilon))}{N} \tag{28}$$

Such that:

- $\text{card}(\arg(|SG_{SB,i} - 0| < \varepsilon))$ refers to the measure of the number of elements having $SG_{SB,i}$ around zero, in other terms $|SG_{SB,i} - 0| < \varepsilon$.
- ε refers to the similarity error ranged in the interval $[10^{-6}, 10^{-4}]$.
- N is the number of the threefold $\{L_1, L_2, e\}$ combinations.

3. Results and Discussion

This section presents the most significant findings in terms of $SBPar$ length computations and modeling according to the decision variables (L_1, L_2, e). The comparison of both L_{SBPar} and L_{SB} to the other benchmark strategies is then straightforward, and it is discussed in light of the resulting specific gain per surface unit values. Moreover, an arbitrary minimization objective was adopted in order to point out the contrast of length between the competing scan strategies. Subsequently, the feasibility of minimal $SBPar$ or SB was studied as a percentage of (L_1, L_2, e) population that fit the negativeness of SG indicators; otherwise, the skeletal scan will show a higher scan trajectory length. Meanwhile, $SBPar$ and SB similarities are discussed according to the computation in expression (10).

According to the method section, the parameters of Table 2 are adopted for the case study.

* L_1 and L_2 are generated according to the procedure (4);

Parameter*	Unity	Designation	Range
L_1	mm	Rectangle length	[100, 300]
L_2	mm	Rectangle width	[50, 250]
e	μm	Hatch space	[25, 1000]

Table 2. Decision parameters and the corresponding ranges.

3.1. SBPar length modeling

In this section, the $SBPar$ length was computed according to all (L_1, L_2, e) combinations. Figure 6 a) depicts the evolution of L_{SBPar} according to (L_1, L_2) and parametrized by the hatch space e. A stepwise modeling of L_{SBPar} according to (L_1, L_2) and e allowed describing and revealing the following behaviors:

- Perfect linear match of the $SBPar$ length according to (L_1, L_2); the coefficients of determination R^2 ranged from 97.34% (at $e = 96.50\,\mu$m) to 97.37% (at $e = 82.50\,\mu$m) with a coefficient of variation (CV) of 0.0055% expressing a significant concentration of R^2 around the 97.35% line. The fitting p-values are found to be less than 10^{-100} levels; Figure 6 b) displays the resulting R^2. Hence, bi-linear models were proposed for each hatch space e as presented by the model (3). In this model, the hatch space e is considered as a parameter instead of a variable as it will be proposed in the second point:

$$L_{SBPar}(L_1, L_2)_e = b_0(e) + b_1(e)L_1 + b_2(e)L_2 \tag{3}$$

Such that, for each surface $L_{SBPar}(L_1, L_2)_e$: - $b_0(e)$ is the y-intercept of the $L_{SBPar}(L_1, L_2)_e$ linear model; - $b_1(e)$ is the slope of the $L_{SBPar}(L_1, L_2)_e$ regression function regarding the L_1 variable; - $b_2(e)$ is the slope of the $L_{SBPar}(L_1, L_2)_e$ regression function regarding the L_2 variable.

- A complex character of L_{SBPar} according to the hatch space e was also observed. Indeed, from the preliminary fitting tests of $\{b_0, b_1, b_2\}$ according to the hatch space e, it was remarkable that $\{b_1, b_2\}$ are perfect hyperboles, and $\{b_0\}$ follows a power-law relation with the hatch space. These behaviors are described by models reported in Table 3 that showed high-quality fitting statistics; Figure 7 depicts the behavior of $\{b_0, b_1, b_2\}$ according to the hatch space e.

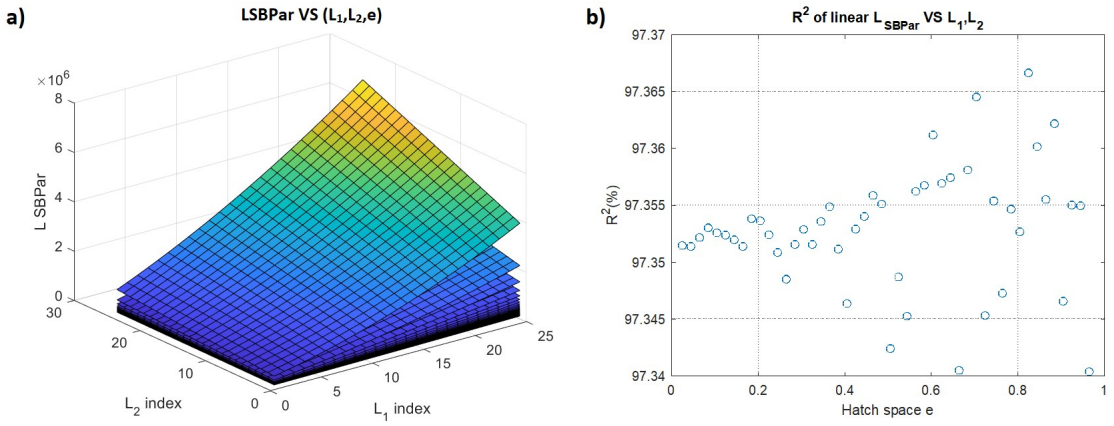

Figure 6. L_{SBPar} vs (L_1, L_2, e)

From a rigorous standpoint, it is noteworthy to emphasize that the perfect fittings are due to the pre-determined analytical formulation of L_{SBPar} according to $\{L_1, L_2, e\}$ that is reported in (19.1) and (19.2); from a statistical standpoint, even if L_{SBPar} involves floor expressions of L_2 and e, it was well-modeled since the number of points is around 50, which allowed a significant statistical modeling.

Finally, based on expressions (30) to (32), one can infer a complete estimation of L_{SBP} according to $\{L_1, L_2, e\}$

with a perfect statistical accuracy as it is proposed by equation (33) and the constant (34); in this expression, the hatch space e is involved as a variable no longer as a parameter.

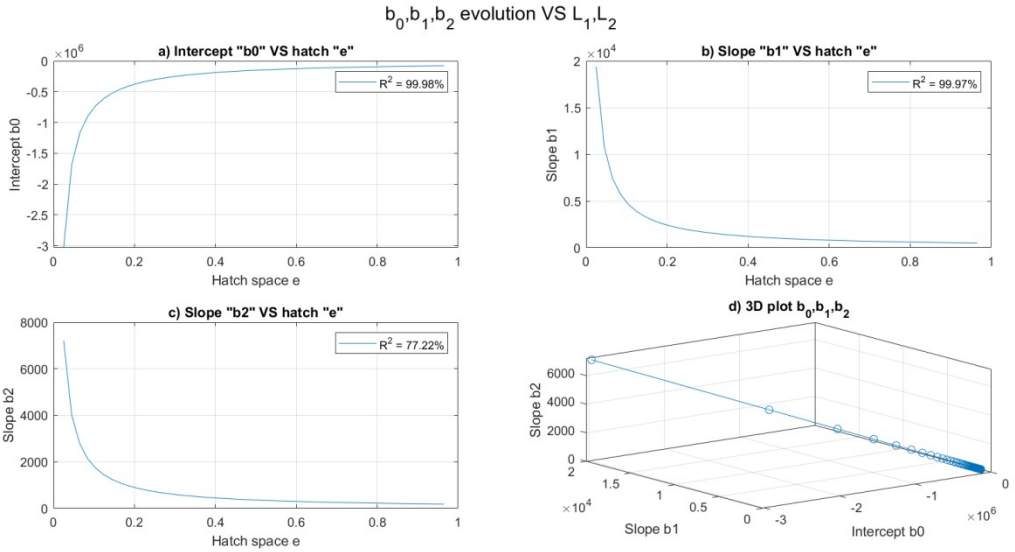

Figure 7. L_{SBPar} vs (L_1, L_2, e)

Model expression	R^2	p-value	Equation index
$b_0(e) = (3.158 \times 10^6)e^{0.115} - 3 \times 10^6$	73.22%	1.84×10^{-14}	(30)
$b_1(e) = \frac{485.01}{e}$	99.99%	2.21×10^{-166}	(31)
$b_2(e) = \frac{180.02}{e}$	99.99%	9.64×10^{-148}	(32)

Table 3. $\{b_0, b_1, b_2\}$ vs $\{e\}$ models.

Typically, identical variations were observed regarding the benchmark strategies lengths namely $\{L_{ch}, L_{st}, L_{sp}, L_{cont}, L_{SBP}\}$ inasmuch as equation (33) is able to describe the benchmark scan lengths according to $\{L_1, L_2, e\}$. Thus, Table 4 consolidates all data regarding the modeling of scan lengths with the corresponding constants; $\{b_0, b_1, b_2\}$ vs $\{e\}$ curves are reported in Appendix in Figures 14 to 17, while L_{SBP} is fully studied in the previous paper [15].

$$L_{SBPar}(L_1, L_2, e) = \alpha_0 e^{\beta} + \alpha_1 \frac{L_1}{e} + \alpha_2 \frac{L_2}{e} \tag{33}$$

$$\begin{cases} \alpha_0 = 3.158 \times 10^6 \,\text{mm}^{1-\beta} \\ \beta = 0.0115 \\ \alpha_1 = 485.01 \,\text{mm} \\ \alpha_2 = 180.02 \,\text{mm} \end{cases} \tag{34}$$

Strategy	α_0	β	α_1	α_2
L_{ch}	1.1684	5.7640	318.6063	136.0372
L_{st}	1.1683	6.3089	549.4448	227.9481
L_{sp}	1.1675	5.6617	287.6499	135.3651
L_{cont}	–	8.1520	3.470×10^3	20.7210

Table 4. Modeling constants of $\{L_{ch}, L_{st}, L_{sp}, L_{cont}, L_{SBP}\}$ vs e according to expression (14).

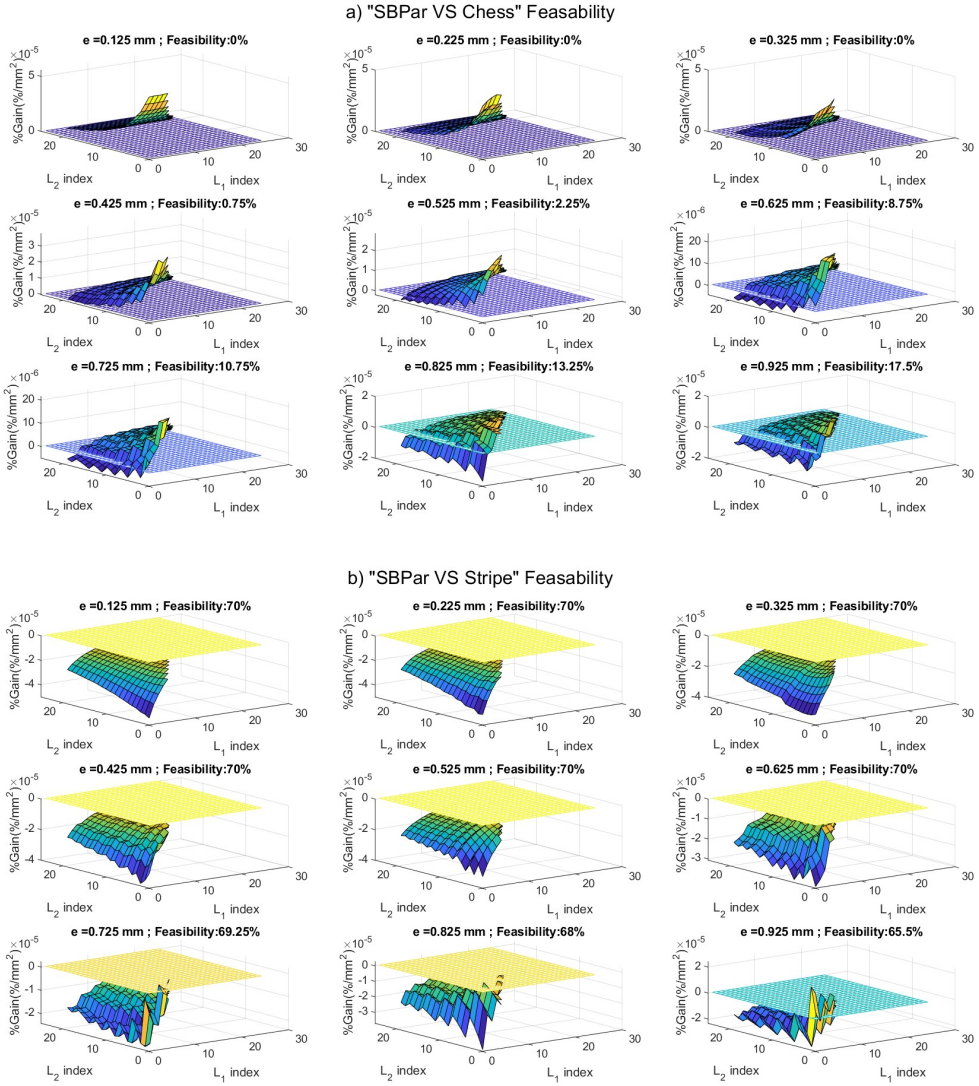

3.2. SBPar Length Comparison

This section comprises a straightforward use of the SG indicators for pairwise comparison of L_{SBPar} to the benchmark strategies. Hence, with regard to the scan length minimization objective, the feasible space is represented by the $\{L_1, L_2, e\}$ areas according to which the corresponding $SG_{SBPar,j}$ is negative. Figure 8.1 to 8.5 display the scan lengths' plots for stepwise increasing values of the hatch space.

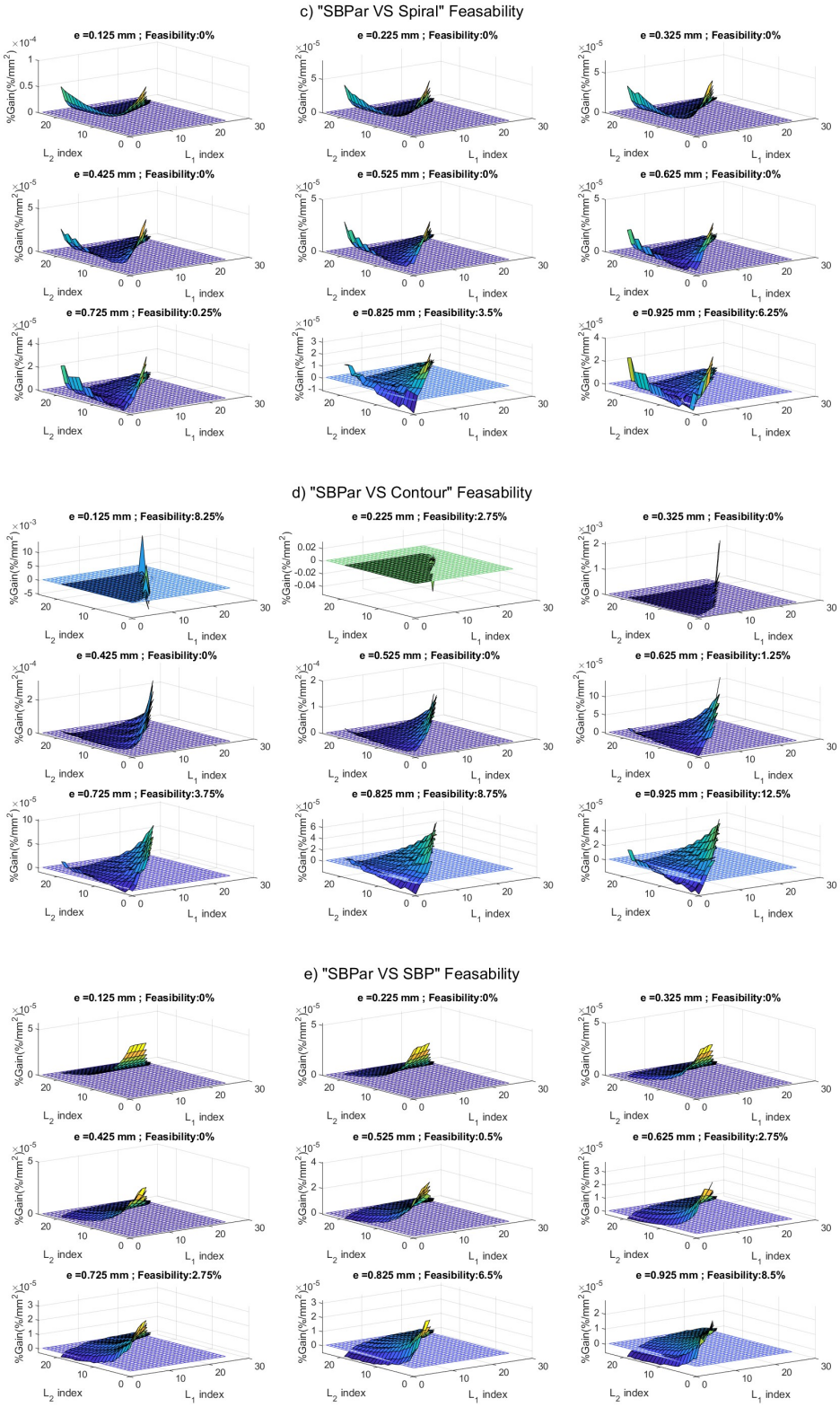

Figure 8. Feasibility areas of L_{SBPar} compared to benchmark scan strategies: a) Chess, b) Stripe, c) Spiral, d) Contour, e) SBP.

Considering the negative zones of the SGs as an arbitrary choice for scan strategies comparisons, Figure 8.a to Figure 8.e allow highlighting the competitiveness of minimal SBPar scan. Based on these figures, it was observed that SBPar can be considered somehow competitive compared to the stripe strategy; but regarding the other benchmark scans, the SBPar length minimization "seemed to be somehow" far from optimality. That is to say, SBPar better maximizes the scanned lengths and then can be considered better controlling the rectangle's area.

To corroborate this discussion, the feasibility percentages were computed by dividing the count of negative SG values by the total number of $\{L_1, L_2, e\}$ combinations. Figure 9 displays the feasibility rates regarding SBPar minimization (Figure 9.a) and SBPar maximization considered as the inverse aspect of SBPar maximization (Figure 9.b). According to these figures, one can observe that the SBPar strategy shows either minimal or maximal trajectory compared to different strategies.

Number of observations can be derived:

- Regarding the total minimization feasibility (Figure 9.a), the SBPar scan seems to be competitive at approximately 70% compared to the stripe strategy, especially for hatch spaces lower than 0.8 mm.
- For the rest of the benchmark strategies $\{L_{ch}, L_{sp}, L_{cont}, L_{SBP}\}$, SBPar minimization feasibility ranged from 0% to 25%, depending on the strategy and the hatch space value. For instance, as for chess, spiral, and contour scans, SBPar showed maximal length until 0.4 mm, starting from which SBPar feasibility started to be better, or in other terms, from which the SBPar started to be competitive from a minimization length perspective.
- The curves of Figure 9.b constitute the complementary profiles of the curves of Figure 9.a. Figure 9.b curves should be regarded as SBPar maximization trajectory performance compared to the benchmark strategies. The same observations can be emphasized as discussed in the first part of the present paragraph.

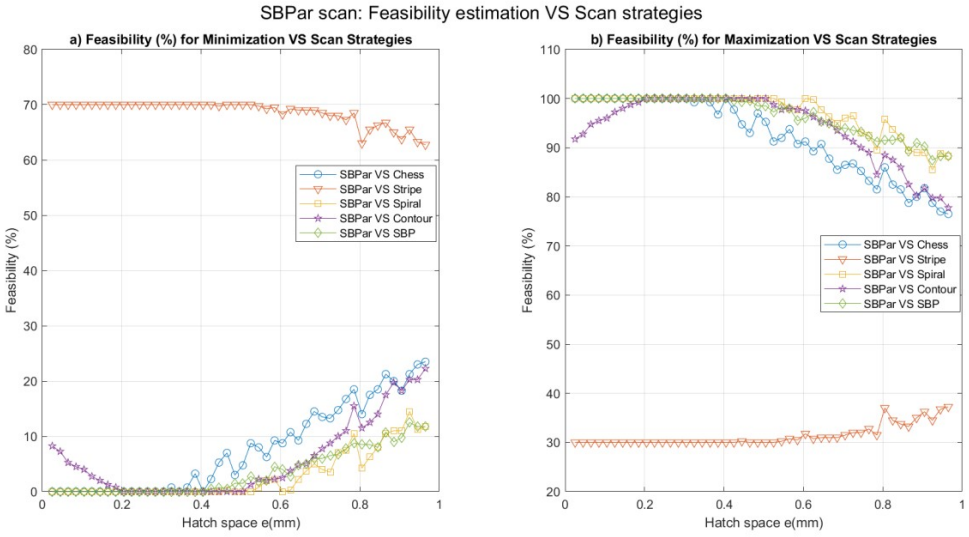

Figure 9. Feasibility percentages of a) SG negativeness regarding L_{SBPar} minimization target, b) SG positiveness regarding L_{SBPar} maximization target.

3.3. Skeleton Based (SB) Scanning Comparison

The Skeleton Based scanning is considered as the complete pattern proposed in this series of works. The SB scan gathers stacks of SBPar and the SBP strategies, SBP layer by SBPar layer and pairs upon pairs, till building the final part; the rectangle shape was adopted herein as a proof of concept of Skeletal scan as introduced earlier. In other terms, the original SB pattern is constituted in basis of two main layers. That is to say, in this section, the

SB total length will be compared to two layers of each benchmark strategy. Subsequently, as presented in Section 2.3, the feasibility analysis is based on the SGs criteria as displayed by expressions (26) and (27), depending on whether minimization or maximization objectives are targeted. The SB minimal scan feasibility will be assigned to negative values of SG_{SB}, while the inverse situation corresponds to SG_{SB} length maximization feasibility.

Figure 10 visually depicts the evolution of the $SG(\%/\text{mm}^2)$ values, emphasizing the negative and positive positions regarding the trifold combinations $\{L_1, L_2, e\}$. Figure 11 completes the feasibility study according to the hatch space e. Similarly to the SG_{SBPar}, the minimization SG_{SB} feasibility is computed by counting the number of negative or positive SG_{SB} points related to the total number of $\{L_1, L_2, e\}$ combinations used in these calculations.

By contrasting the curves of Figure 10 and Figure 11, it is noteworthy that the act of constructing the total SB length by SBPar and SBP superposition does not highly affect the skeletal-based scan SB performances compared to the stripe scan; indeed, the feasibility at minimization is still fluctuating around 70%, and a slight enhancement of 2% was denoted at hatch spaces exceeding 0.8 mm. Meanwhile, the SB enhanced the minimization feasibility compared to SBPar regarding the rest of the benchmark strategies {Chess, Spiral, Contour}. This evolution starts around 0.3 mm of hatch space and evolves linearly from an enhancement of 4% at hatch space 0.3 mm to reaching 10% around a hatch space of 1 mm, as highlighted in Figure 11a.

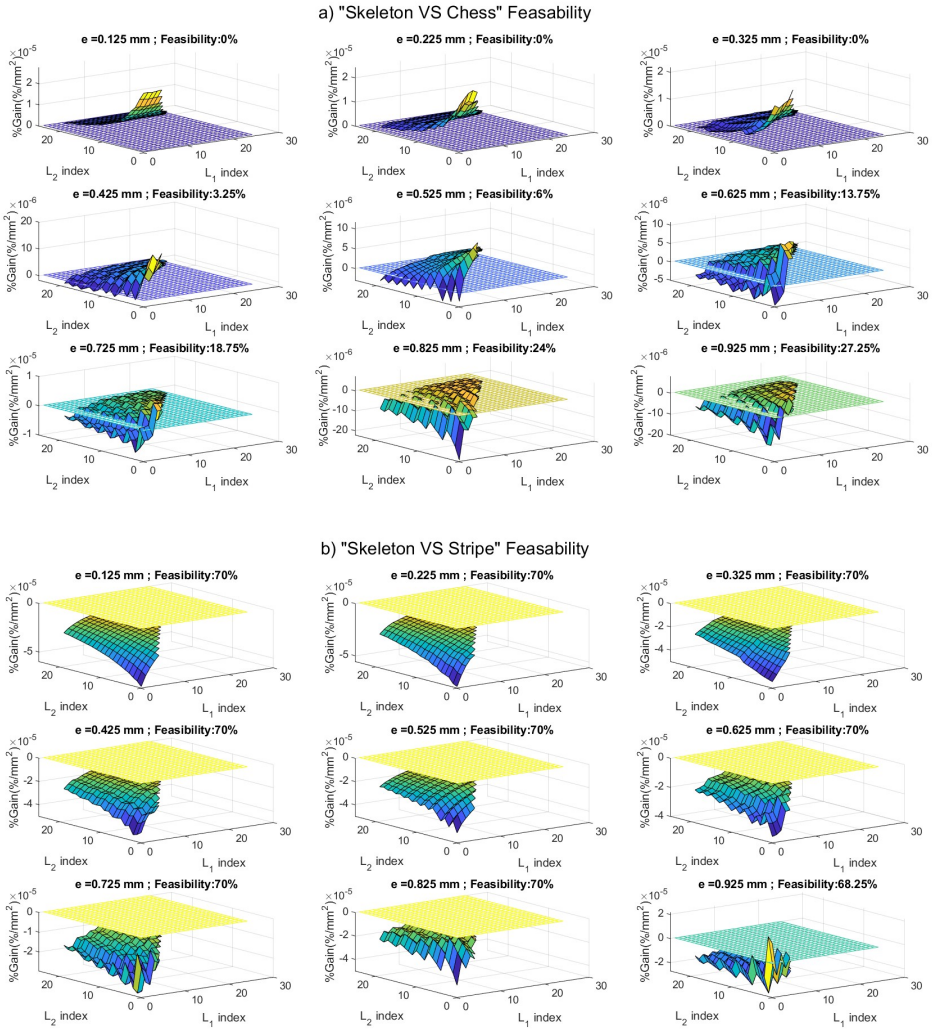

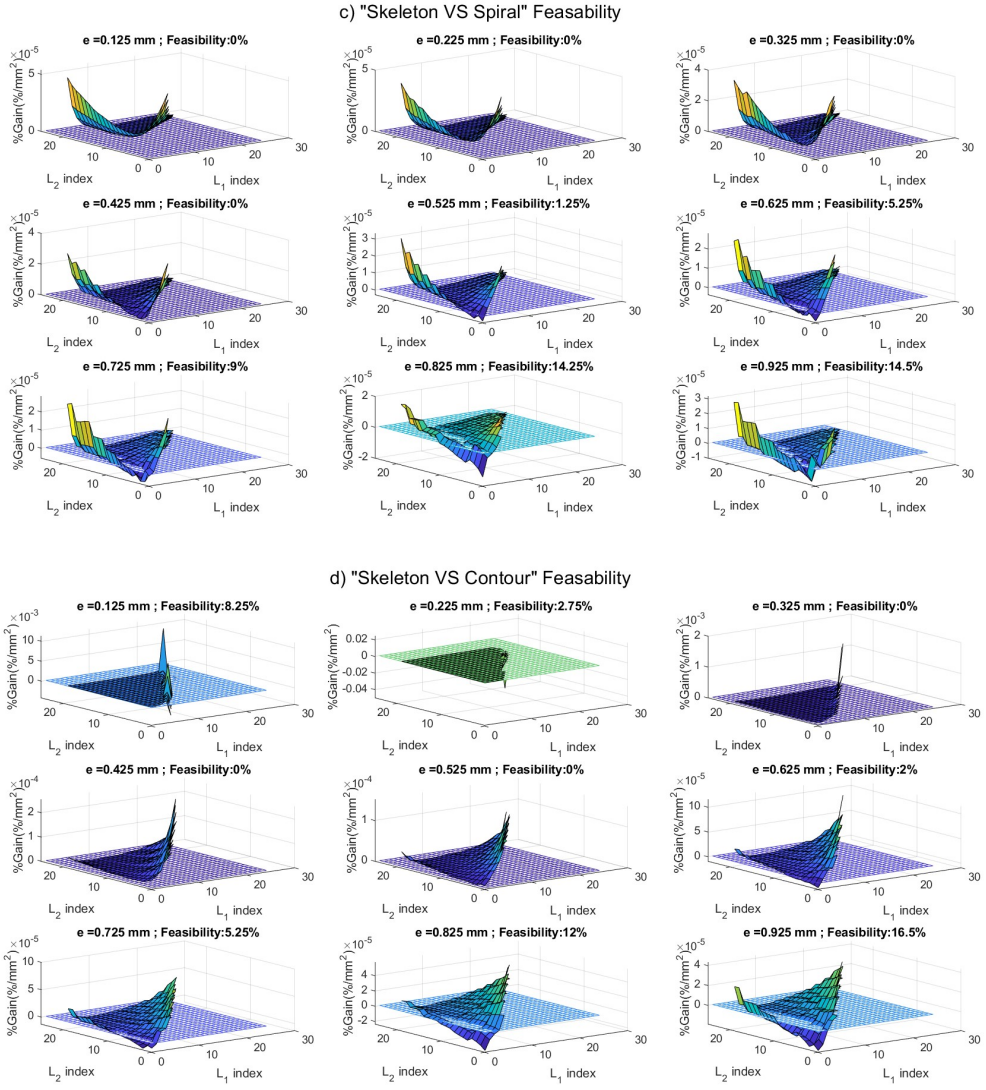

Figure 10. Feasibility areas of L_{SB} compared to benchmark scan strategies: a) Chess, b) Stripe, c) Spiral, d) Contour, e) SBP.

3.4. SB Similarity Assessment

An additional analysis consists in finding similarities between the designed total SB scan and the benchmark strategies in terms of null values of the SG indicators. Indeed, according to expressions (21) to (25), at equal scan lengths, the SG indicator falls to zero, so that the corresponding competing scan shows similar length values Sim(%). Thus, SB scan similarities to the benchmark hatching patterns are assessed according to expression (10).

According to Figure 12, it is salient that the similarity values behave as an exponential or a power-law of error of similarity ε for all pairwise similarity assessments {SB, Benchmark scan}.

In this assessment, the similarity tolerance ε was varied from 10^{-6} to 10^{-4} to capture the similarity variation accuracy Sim(%) and the corresponding eventual convergence, if it exists. For instance, according to Figure 12, SB similarity to chess, spiral, and stripe patterns reached 70% at respective errors of 2×10^{-5}, 4×10^{-5}, and 4.5×10^{-5}, while the contour strategy seems to be far from similar to SB with a maximum similarity of 63% for a

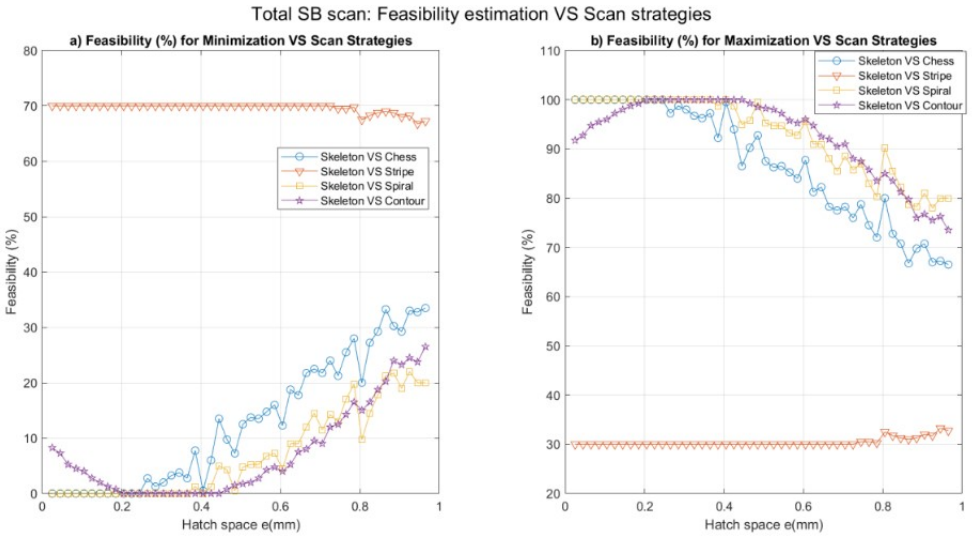

Figure 11. Feasibility percentages of a) SG_{SB} negativeness regarding L_{SB} minimization objective, b) SG_{SB} positiveness regarding L_{SB} maximization objective.

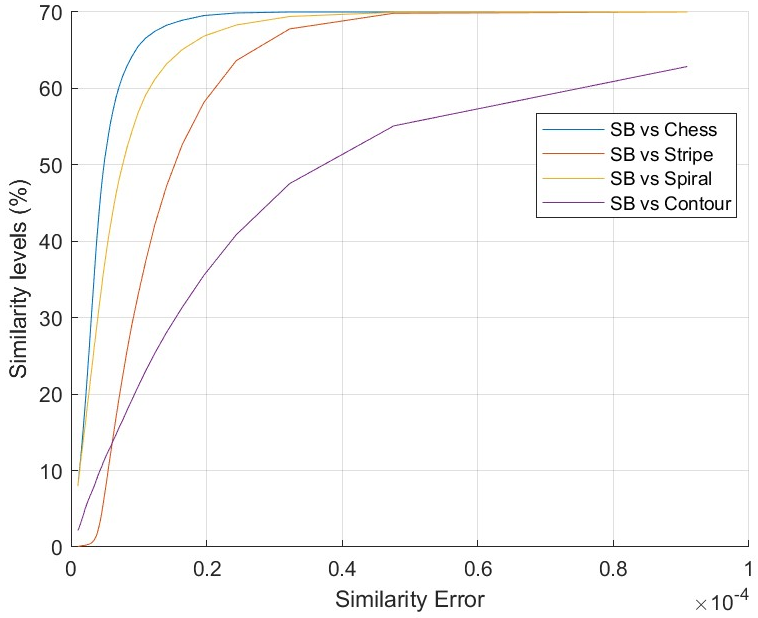

Figure 12. Similarities of SB vs benchmark hatching patterns as a function of similarity error.

high error value near 1×10^{-4}. Similarly, Figure 12 curves can be differently read at a fixed value in the y-axis; for instance, fixing a given similarity refers to different errors ε for different benchmark hatching strategies. For more practical findings' exploitation, equation (35) proposed herein describes the regressive similarity models according to the similarity tolerance with the corresponding fitting statistics that are exhibited in Table 5.

According to a series of models tests, exponential models showed very high accuracy compared to power-law; the adopted model corresponds to SB similarity "sim(%)" as a function of similarity tolerance ε as depicted by

expression (35); the resulting optimal fitting parameters (K^*, t^*) and R^2 statistics are reported in table 5. These significant findings are corroborated by Figure 13 which can graphically attest the high quality if the first-order exponential models adopted herein.

$$\text{sim}(\%) = K(1 - e^{-t\cdot\varepsilon}), \quad \varepsilon \in [10^{-6}, 10^{-4}], \quad K, t > 0 \tag{35}$$

Comparison	K^* (Mean)	Confidence Bounds†	t^* (Mean)	Confidence Bounds†	$R^2(\%)$
SB vs Chess	76.14	[72.45, 79.82]	1.652×10^5	$[1.506 \times 10^5, 1.798 \times 10^5]$	95.23
SB vs Stripe	88.00	[73.34, 102.7]	3.341×10^4	$[2.459 \times 10^4, 4.223 \times 10^4]$	85.84
SB vs Spiral	73.16	[71.54, 74.79]	1.312×10^5	$[1.261 \times 10^5, 1.364 \times 10^5]$	99.03
SB vs Contour	65.57	[64.93, 66.22]	3.872×10^4	$[3.811 \times 10^4, 3.933 \times 10^4]$	99.91

Table 5. Similarity model vs error of similarity (Equation 35)

†95% Confidence Bounds.

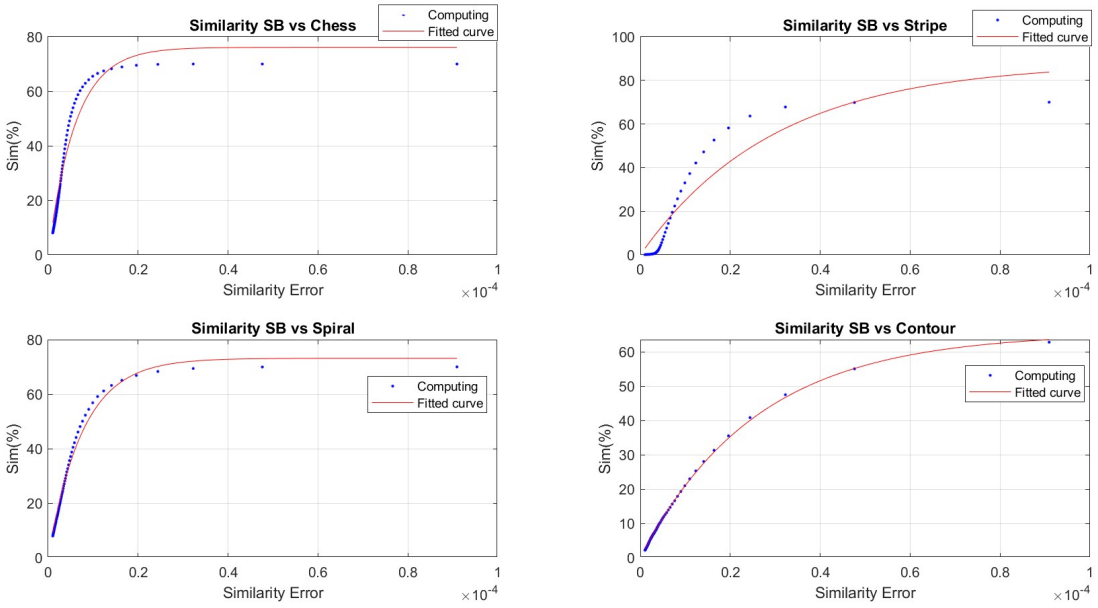

Figure 13. Similarities fitting of SB vs benchmark hatching patterns as a function of similarity error ε.

4. Conclusion

This paper is the second one of a series of research works that aims at establishing a rigorous basement of Skeleton Based (SB) scan strategy. The first paper designed the Skeleton Based Perpendicular (SBP) as a minimal trajectory hatch pattern [15]; the proof of concept was applied to a simple geometry, namely a rectangle $(L_1, L_2)_{(L_1>L_2)}$. In the present work, the author designed the SBP complementary scan namely the Skeleton Based Parallel in order to balance the eventual anisotropy that should be brought by the SBP scan. That is to say, the SB scan is composed of a superposition of pairwise couple of layers (SBP; SBPar). Then, it is worth recalling, that this paper rigorously and stepwise draws-up the main geometrical features and characteristics, in terms of salient points, principal intersections, bisectors, and so forth as it was displayed in the Mathematical developments of Section 2.

Subsequently, this paper involves the SBPar length and the SB total length as main features to be compared to benchmark strategies; the competing hatching includes chess, stripe, spiral, and contour that were already utilized in the SBP paper [15]. As for the comparison basis, the specific gain per surface unit (SG) was adopted; this indicator allows comparing the difference of peer-to-peer scan lengths per surface area $(L_1 \times L_2)$ of the proposed design to the scan benchmark strategies. Furthermore, the comparison dealt with both minimization of maximization of the scan total length in the present analysis; then, the length minimization was discussed as an arbitrary classical optimization strategy to be reached by the new design. In another hand, the author included scans' similarity assessment that is based on a similarity indicator; this latter was computed for different similarity tolerance ε ranging between 10^{-6} and 10^{-4}.

According to the findings of this research, number of conclusions are derived:

- The SBPar total scan length L_{SBPar} behaves linearly regarding the rectangle dimensions $\{L_1, L_2\}$.
- As for the hatch space parameter e, $L_{SBPar}(e)$ was observed to be a superposition of a power-law $\sim e^{\beta}, \beta > 0$ and a hyperbole $\sim 1/e$.
- Regarding the SG indicator, both SBPar and SB pattern show:
  - Minimal trajectory compared to the stripe strategy.
  - Maximal trajectory compared to the chess, spiral, and contour hatching.
- Similarities between scan lengths were also assessed around the zero line of the SG indicators; the zero line was considered in this analysis as a convergence line of similar patterns of pair scans strategies to be compared. The similarity percentage sim(%) was found to fit a perfect exponential first-order behavior according to the estimation tolerance ε. It was found that the skeletal total scan SB can reach up to 70% of similarity with the stripe strategy and less than 20% for the rest of the patterns. A wide choice of parameters values $\{L_A, L_3, e\}$ can then be analyzed depending on whether designers are looking for pattern trajectory maximization or minimization.

Therefore, the present study tries to gather all the required information about scan length of the general Skeleton Based scanning SB. Moreover, it was highlighted that the maximization of the scan length, compared to other hatching strategies, can be promoted as a design which allows maximal controlling the scanned area, inasmuch as users have to maximize matter density, leading to parts strengthening or other specific physical objectives are needed by the designers. In such cases, the feasibility criterion of expression (27) involves optimal $\{L_1^{(**)}, L_2^{(**)}, e^{(**)}\}$ combinations regarding a L_{SBPar} maximization policy, and feasibility curves of Figure 9.b and Figure 11.b are to be adopted for $\{L_1, L_2, e\}$ parameters selection.

Finally, it is worth mentioning that the third work of this series of research will focus on gcode design of both SBP and SBPar implementation within 3D printers; the aim is to compare 3D-printed parts properties, especially the mechanical anisotropy, to existing hatching strategies. Other features such as material's density and layers cohesions are also to be assessed in future investigations; while the SBPar geometry is now exploited as the basis of a novel heat sink newly designed for the electronic circuit for enhancing surface heat exchange [66].

Appendix – Benchmark Strategies Lengths Models Parameters $\{b_0, b_1, b_2\}$ vs $\{e\}$

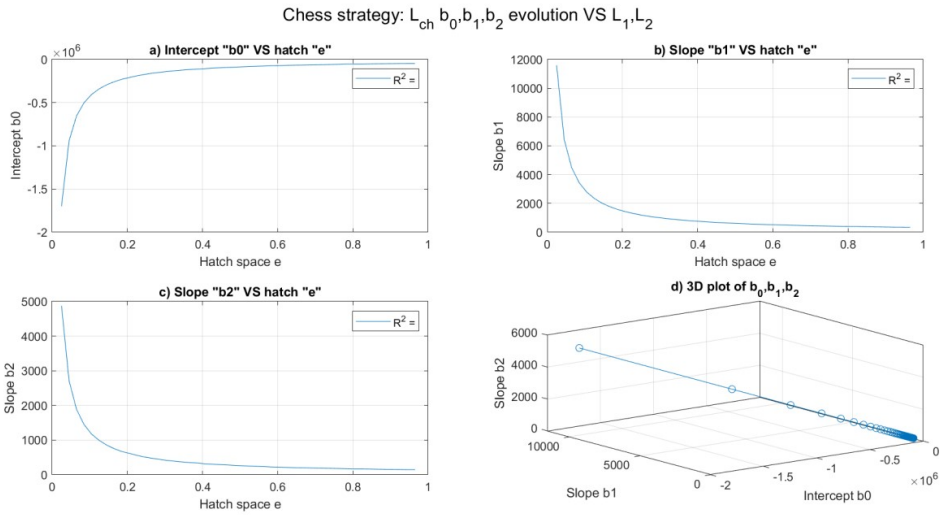

Figure 14. Chess scan Length L_{ch} linear modeling parameters $\{b_0, b_1, b_2\}$.

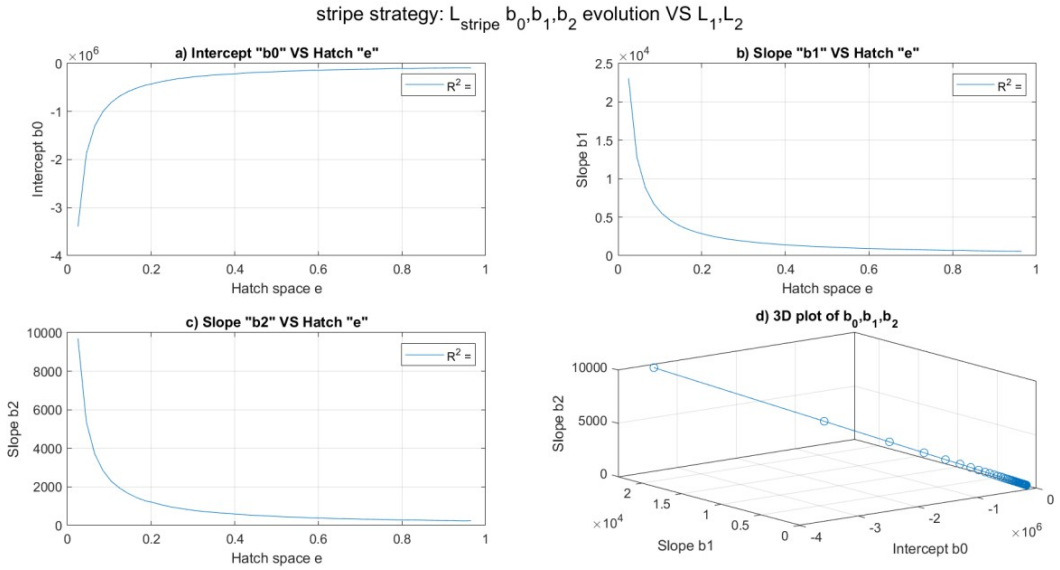

Figure 15. Stripe scan Length L_{st} linear modeling parameters $\{b_0, b_1, b_2\}$.

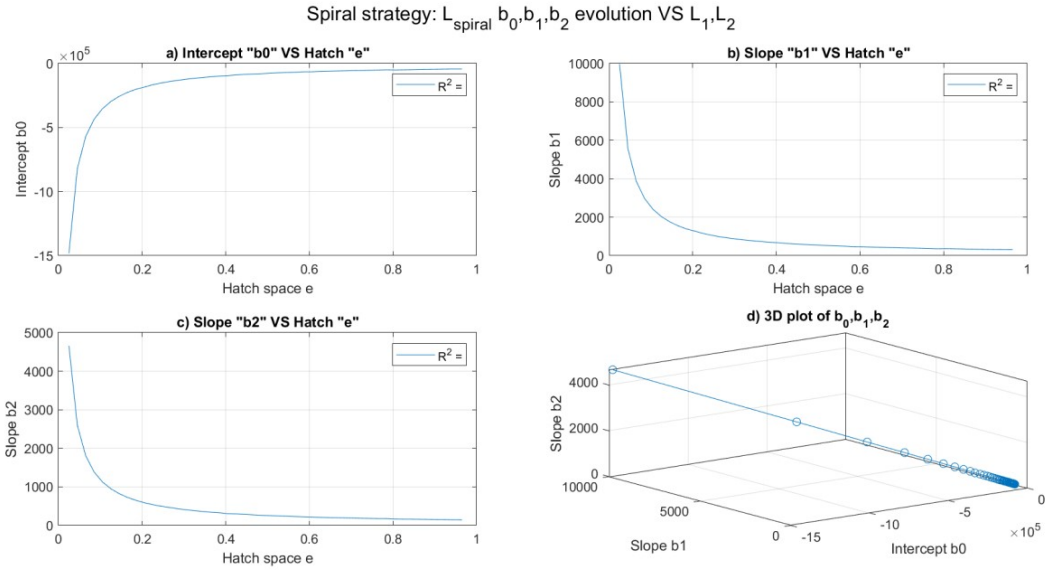

Figure 16. Spiral scan Length L_{sp} linear modeling parameters $\{b_0, b_1, b_2\}$.

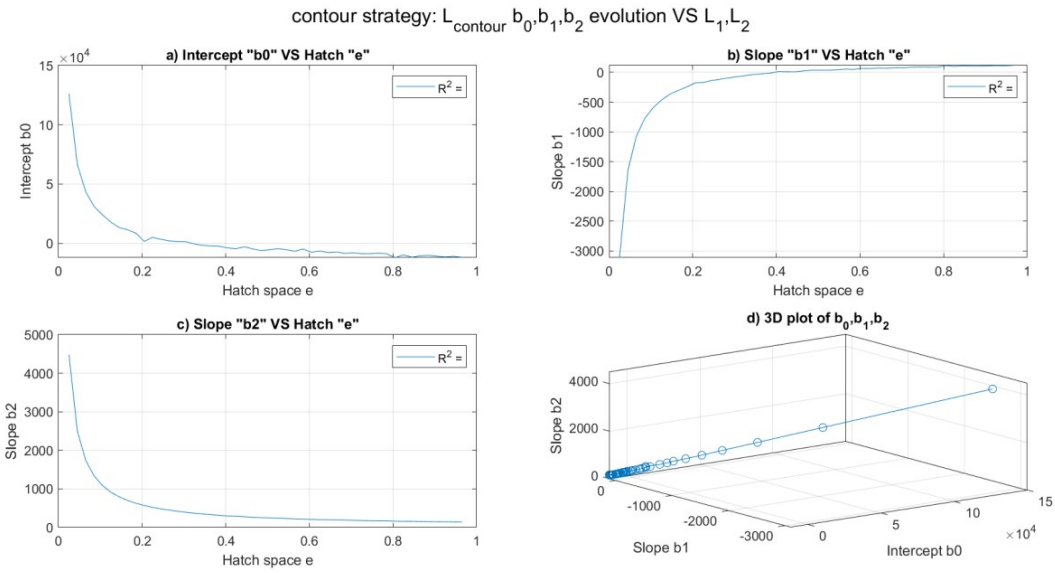

Figure 17. Contour scan Length L_{cont} linear modeling parameters $\{b_0, b_1, b_2\}$.

REFERENCES

1. S Torta and J Torta. *3D Printing: An Introduction.* Mercury Learning and Information, Dulle, Massachusetts, USA, 2019.
2. K. Ouazzani, M. E. Jai, B. Elfahime. *Detailed classification of FDM (Fused Deposition Modeling) process parameters and potentially affected part characteristics.* In: 2022 2nd International Conference on Innovative Research in Applied Science, Engineering and Technology (IRASET), Meknes, Morocco, 2022, pp. 1–9. doi:10.1109/IRASET52964.2022.9738432

3. Ouazzani K., Akhrif I., Rihani N., El Jai M., Radouani M., El Fahime B. *Processing Parameters, Heat-Treatment, and Testing Speed influence on Tensile properties of ABS-FDM materials.* Mor. J. Chem., 12(4), 1621–1663 (2024).
4. K Fri, A Laazizi, M Bensada, et al. *Microstructural and heat treatment analysis of 316L elaborated by SLM additive manufacturing process.* Int J Adv Manuf Technol, 124, 2289–2297 (2022). https://doi.org/10.1007/s00170-022-10622-4
5. K Fri, I Akhrif, A Laazizi, et al. *Experimental investigation of the effects of processing parameters and heat treatment on SS 316L manufactured by laser powder bed fusion.* Prog Addit Manuf. (2023). https://doi.org/10.1007/s40964-023-00538-0
6. H.M. Alzahrani. *In silico study of the electronic portal imaging devices sensitivity to parotid glands shrinkage during radiotherapy for nasopharyngeal cases.* J.Umm Al-Qura Univ. Appl. Sci. 10, 279–289 (2024). https://doi.org/10.1007/s43994-023-00103-z
7. K. Ouazzani, M. E. Jai, I. Akhrif, M. Radouani, B. Elfahime. *Minimization of Surface Roughness for ABS Specimens Relatively to FDM Process Parameters - an Experimental Analysis.* In: 2024 4th International Conference on Innovative Research in Applied Science, Engineering and Technology (IRASET), FEZ, Morocco, 2024, pp. 1–5. doi:10.1109/IRASET60544.2024.10548529
8. S Roux, Le M Salem, A Hor. *Improvement of the bridge curvature method to assess residual stresses in selective laser melting.* Addit Manuf, 22, 320-329 (2018). https://doi.org/10.1016/j.addma.2018.05.025
9. M Yakout, M.A. Elbestawi, S.C. Veldhuis. *Density and mechanical properties in selective laser melting of Invar 36 and stainless steel 316L.* J Mater Process Technol. (2018). https://doi.org/10.1016/j.jmatprotec.2018.11.006
10. D Pitassi, et al. *Finite element thermal analysis of metal parts additively manufactured via selective laser melting.* In: P Răzvan (ed) Finite element method: simulation, numerical analysis and solution technique. IntechOpen, 123–156 (2018).
11. J Suryawanshi, K.G. Prashanth, U Ramamurty. *Mechanical behavior of selective laser melted 316L stainless steel.* Mater Sci Eng A, 696, 113-121 (2017). https://doi.org/10.1016/j.msea.2017.04.058
12. J Damon, S Dietrich. *Process porosity and mechanical performance of fused filament fabricated 316L stainless steel.* Rapid Prot J, 25(7), 1319-1327 (2019). https://doi.org/10.1108/RPJ-01-2019-0002
13. A Kudzal. *Effect of scan pattern on the microstructure and mechanical properties of Powder Bed Fusion additive manufactured 17–4 stainless steel.* Mater Design, 133, 205-215 (2017). https://doi.org/10.1016/j.matdes.2017.07.047
14. S Catchpole-Smith. *Fractal scan strategies for selective laser melting of 'unweldable' nickel superalloys.* Add Man, 15, 113-122 (2017). https://doi.org/10.1016/j.addma.2017.02.002
15. El Jai, M., Saidou, N., Zineddine, M. et al. *Mathematical design and preliminary mechanical analysis of the new lattice structure: "GE-SEZ*" structure processed by ABS polymer and FDM technology.* Prog Addit Manuf, 6, 93–118 (2021). https://doi.org/10.1007/s40964-020-00148-0
16. T Mishurova, K Artzt, J Haubrich. *New aspects about the search for the most relevant parameters optimizing SLM materials.* Addit Manuf, 25, 325-334 (2018). https://doi.org/10.1016/j.addma.2018.11.023
17. Bähr, M., Buhl, J., Radow, G., et al. *Stable honeycomb structures and temperature-based trajectory optimization for wire-arc additive manufacturing.* Optim Eng, 22, 913–974 (2021). https://doi.org/10.1007/s11081-020-09552-5
18. D Gu, H Chen. *Selective laser melting of high strength and toughness stainless steel parts: the roles of laser hatch style and part placement strategy.* Mater Sci Eng A, 725, 419-427 (2018). https://doi.org/10.1016/j.msea.2018.04.046
19. M El Jai, I Akhrif, & N Saidou. *Skeleton-based perpendicularly scanning: a new scanning strategy for additive manufacturing, modeling and optimization.* Prog Addit Manuf, 6, 781–820 (2021). https://doi.org/10.1007/s40964-021-00197-z
20. E.O. Olakanmi, R.F. Cochrane, K.W. Dalgarno. *Densification mechanism and microstructural evolution in selective laser sintering of Al–12Si powders.* J Mater Process Technol, 211, 113-121 (2011). https://doi.org/10.1016/j.jmatprotec.2010.09.003
21. H. Gong. *Influence of defects on mechanical properties of Ti–6Al–4V components produced by selective laser melting and electron beam melting.* Mater Design, 86, 545-554 (2015). https://doi.org/10.1016/j.matdes.2015.07.147
22. Fri, K., Laazizi, A., Akhrif, I., Jai, M.E., Ouannou, A., Bensada, M. *Metallurgical Study of a Material Produced by Selective Laser Melting.* In: Azrar, L., et al. *Advances in Integrated Design and Production II. CIP 2022. Lecture Notes in Mechanical Engineering.* Springer, Cham (2023). https://doi.org/10.1007/978-3-031-23615-0_51
23. M. Yakout, M.A. Elbestawi, S.C. Veldhuis. *A study of thermal expansion coefficients and microstructure during selective laser melting of Invar 36 and stainless steel 316L.* Addit Manuf, 24, 405-418 (2018). https://doi.org/10.1016/j.addma.2018.09.035
24. K. Easterling. *Introduction to the Physical Metallurgy of Welding.* Butterworth-Heinemann, 2nd Edition, Great Britain, 1992.
25. C. Wu, S. Li, C. Zhang, X. Wang. *Microstructural evolution in 316LN austenitic stainless steel during solidification process under different cooling rates.* J Mater Sci, 51, 2529-2539 (2016). https://doi.org/10.1007/s10853-015-9565-0
26. A.F. Padilha, & P.R. Rios. *Decomposition of Austenite in Austenitic Stainless Steels.* ISIJ International, 42(4), 325–337 (2002). https://doi.org/10.2355/isijinternational.42.325
27. D. Kong. *Heat treatment effect on the microstructure and corrosion behavior of 316L stainless steel fabricated by selective laser melting for proton exchange membrane fuel cells.* Electrochim Acta (2018). https://doi.org/10.1016/j.electacta.2018.04.188
28. D. Kong. *Anisotropy in the microstructure and mechanical property for the bulk and porous 316L stainless steel fabricated via selective laser melting.* Mater Lett, 235, 1-5 (2019). https://doi.org/10.1016/j.matlet.2018.09.152
29. J.-C. Lippold, D.-J. Kotecki. *Welding metallurgy and weldability of stainless steels.* John Wiley & Sons Publication, New Jersey, USA, 2005.
30. Oulkhir, F., Akhrif, I. & El Jai, M. *3D concrete printing success: an exhaustive diagnosis and failure modes analysis.* Prog Addit Manuf, 10, 517–559 (2025). https://doi.org/10.1007/s40964-024-00638-5
31. Oulkhir, F.Z., Rihani, N., Akhrif, I. & El Jai, M. *Integration of Earth-based materials in 3D concrete printing (3DCP): Physico-chemical and Technological characterization.* E3S Web Conf., **601**, 00024 (2025). https://doi.org/10.1051/e3sconf/202560100024
32. Rihani, N., Oulkhir, F.Z., Igwe, N.C., Akhrif, I. & El Jai, M. *3D Clay Printing: A Taguchi Approach To Rheological Properties And Printability Assessment.* E3S Web Conf., **601**, 00023 (2025). https://doi.org/10.1051/e3sconf/202560100023
33. E. Liverani. *Effect of Selective Laser Melting (SLM) process parameters on microstructure and mechanical properties of 316L austenitic stainless steel.* J Mater Process Technol, 249, 255-263 (2017). https://doi.org/10.1016/j.jmatprotec.2017.05.042
34. K.G. Prashanth, S. Scudino, H.J. Klauss, et al. *Microstructure and mechanical properties of Al-12Si produced by selective laser melting: effect of heat treatment.* Mater Sci Eng A, 590, 153-160 (2014). https://doi.org/10.1016/j.msea.2013.10.023
35. A. Pathania, A.K. Subramaniyan, N. Bommanahalli Kenchappa. *Densification behaviour of laser powder bed fusion processed Ti6Al4V: Effects of customized heat treatment and build direction.* Proceedings of the Institution of Mechanical Engineers. Part E:

Journal of Process Mechanical Engineering (2023). https://doi.org/10.1177/09544089231190483
36. C. Qiu, N.J.E. Adkins, M.M. Attallah. *Microstructure and tensile properties of selectively laser-melted and of HIPed laser-melted Ti-6Al-4V.* Mater Sci Eng A, 578, 230–239 (2013). https://doi.org/10.1016/j.msea.2013.04.099
37. S. Tammas-Williams, P.J. Withers, I. Todd, et al. *Porosity regrowth during heat treatment of hot isostatically pressed additively manufactured titanium components.* Scr Mater, 122, 72–76 (2016). https://doi.org/10.1016/j.scriptamat.2016.05.002
38. K. Ouazzani, M. El Jai, I. Akhrif, et al. *An experimental study of FDM parameter effects on ABS surface quality: roughness analysis.* Int J Adv Manuf Technol, 127, 151–178 (2023). https://doi.org/10.1007/s00170-023-11435-9
39. Igwe, N.C., Akhrif, I., El Jai, M. et al. *An experimental investigation of the influence of SLM input factors on the as-built AlSi10Mg surface quality.* Int J Adv Manuf Technol, **136**, 619–674 (2025). https://doi.org/10.1007/s00170-024-14657-7
40. M.S. Duval-Chaneac. *Experimental study on finishing of internal laser melting (SLM) surface with abrasive flow machining (AFM).* Precis Eng (2018). https://doi.org/10.1016/j.precisioneng.2018.03.006
41. A.H. Mary, T. Kara. *Robust Proportional Control for Trajectory Tracking of a Nonlinear Robotic Manipulator: LMI Optimization Approach.* Arab J Sci Eng, 41, 5027–5036 (2016). https://doi.org/10.1007/s13369-016-2221-4
42. X. Ji, S. Feng, Q. Han, et al. *Improvement and Fusion of A* Algorithm and Dynamic Window Approach Considering Complex Environmental Information.* Arab J Sci Eng, 46, 7445–7459 (2021). https://doi.org/10.1007/s13369-021-05445-6
43. El Abbaoui, K., Al Korachi, I., El Jai, M., Šeta, B. & Mollah, M.T. *3D concrete printing using computational fluid dynamics: Modeling of material extrusion with slip boundaries.* Journal of Manufacturing Processes, **118**, 448–459 (2024). ISSN 1526-6125. https://doi.org/10.1016/j.jmapro.2024.03.042
44. Akhrif, I., Oulkhir, F.Z., El Jai, M. et al. *Earth-based materials 3D printing, extrudability and buildability numerical investigations.* Prog Addit Manuf (2025). https://doi.org/10.1007/s40964-025-01014-7
45. C. Rousseau, & Y. Saint-Aubin. *Mathematiques and technologie.* SUMAT Springer, 2001.
46. P. Felkel, S. Obderzalek. *Straight skeleton implementation.* Reprinted proceedings of Spring Conference on Computer Graphics, 210–218 (1998), Budmerice, Slovakia.
47. W. Zizhao, C. Xingyu, Y. Lingyun, et al. *Co-skeletons: Consistent curve skeletons for shape families.* Computers & Graphics, 90, 62-72 (2020). https://doi.org/10.1016/j.cag.2020.05.006
48. R.L. Blanding, G.M. Turkiyyah, D.W. Storti, M.A. Ganter. *Skeleton-based three-dimensional geometric morphing.* Computational Geometry, 15, 129–148 (2000). https://doi.org/10.1016/S0925-7721(99)00050-4
49. Yuchen He, Sung Ha Kang, & Luis Álvarez. *Finding the Skeleton of 2D Shape and Contours: Implementation of Hamilton-Jacobi Skeleton.* Image Processing On Line, 11, 18–36 (2021). https://doi.org/10.5201/ipol.2021.296
50. Rihani, N., Akhrif, I., El Jai, M. *Proposition and design of a new Micro-Architected Domes family: A biomimicry-based approach.* Frontiers of Architectural Research, **13**(3), 650–667 (2024). ISSN 2095-2635. https://doi.org/10.1016/j.foar.2024.01.004
51. Rihani, N., Akhrif, I., El Jai, M. & Lamghari, M. *Finite Element modeling and convergence analysis of a new Biomimetic Branching Structure.* Statistics, Optim. Inf. Comput., **12**(3), 713–726 (2024). https://doi.org/10.19139/soic-2310-5070-1964
52. Q.J. Wu, & J.D. Bourland. *A morphology-guided radiosurgery treatment planning and optimization for multiple isocenters.* Med Phys, 26, 2151-2160 (1999). https://doi.org/10.1118/1.598731
53. Q.J. Wu. *Sphere packing using morphological analysis.* Ser Discr Math Theor Comput Sci, 55, 45-54 (2000). https://doi.org/10.1090/dimacs/055
54. M.Z. El Khattabi, M. El Jai, Y. Lahmadi, et al. *Understanding the Interplay Between Metrics, Normalization Forms, and Data distribution in K-Means Clustering: A Comparative Simulation Study.* Arab J Sci Eng (2023). https://doi.org/10.1007/s13369-023-07741-9
55. M.Z. El Khattabi, M. El Jai, Y. Lahmadi, et al. *Geometry-Inference Based Clustering Heuristic: New k-means Metric for Gaussian Data and Experimental Proof of Concept.* Oper. Res. Forum, 5, 13 (2024). https://doi.org/10.1007/s43069-024-00291-2
56. El Jai, M., Herrou, B. & Benazza, H. *Integration of a Risk Analysis method with Holonic approach in an Isoarchic context.* Int. J. Eng. Technol., **5**, 5196–5206 (2013).
57. Jai, M., Akhrif, I., Herrou, B. & Benazza, H. *Correction of the Production Master Plan According to Preventive Maintenance Constraints and Equipments Degradation State.* Engineering, **6**, 274–291 (2014). https://doi.org/10.4236/eng.2014.66032
58. Jai, M., Akhrif, I., Abidine, T., Djouma, N.M., Herrou, B., Benazza, H. & Hammoumi, M. *Intelligent process optimization into holonic manufacturing systems using TAGUCHI approach and UML modeling language.* Int. J. Sci. Eng. Res., **6**(5), 1099–1107 (2015).
59. El Jai, M. *Modélisation et Optimisation des systèmes industriels: Paradigme Holonique Optimisation Multiobjectif.* Éditions universitaires européennes (2017).
60. Abassi, A., El Jai, M., Arid, A. et al. *Modeling and Mitigating Billing Attacks in Scalable Smart Grids with Distributed and Intelligent Systems.* Oper. Res. Forum, **6**, 17 (2025). https://doi.org/10.1007/s43069-025-00414-3
61. Abassi, A., Bakkas, B., Jai, M.E., Arid, A. & Benazza, H. *A Multi-Split Cross-Strategy for Enhancing Machine Learning Algorithms Prediction Results with Data Generated by Conditional Generative Adversarial Network.* J. Comput. Sci., **20**(7), 700–707 (2024). https://doi.org/10.3844/jcssp.2024.700.707
62. Abassi, A., El Jai, M., Arid, A. et al. *A Multiscale study of flexible customer's energy demand under smart grid architecture: A modeling and simulation study.* Energy Effic., **17**, 54 (2024). https://doi.org/10.1007/s12053-024-10234-9
63. El Jai, M., Zhar, M., Ouazar, D. et al. *Socio-economic analysis of short-term trends of COVID-19: modeling and data analytics.* BMC Public Health, **22**, 1633 (2022). https://doi.org/10.1186/s12889-022-13788-4
64. Akhrif, O., Benfaress, C., El Jai, M., El Bouzekri El Idrissi, Y. & Hmina, N. *Completeness based classification algorithm: a novel approach for educational semantic data completeness assessment.* Interact. Technol. Smart Educ., **19**(1), 87–111 (2022). https://doi.org/10.1108/ITSE-01-2021-0017
65. J. Schmidt, A. Fügenschuh. *Trajectory optimization for arbitrary layered geometries in wire-arc additive manufacturing.* Optim Eng, 25, 529–553 (2024). https://doi.org/10.1007/s11081-023-09813-z
66. Nimbona, F., Jai, M.E., Akhrif, I. et al. *Simulation-based optimization and parametric identification of a new skeletal shape-based fins' heat exchanger.* J Therm Anal Calorim., 1–39 (2025). https://doi.org/10.1007/s10973-025-14376-5